



# On the solid/liquid interfacial energies of metals and alloys

George Kaptay<sup>1,2,3,\*</sup>

<sup>1</sup>Department of Nanotechnology, University of Miskolc, Egyetemvaros, Miskolc 3515, Hungary

<sup>2</sup>MTA-ME Materials Science Research Group, Egyetemvaros, Miskolc 3515, Hungary

<sup>3</sup>Bay Zoltan Ltd for Applied Research, BAY-ENG, 2 Igloi, Miskolc 3519, Hungary

Received: 10 August 2017

Accepted: 30 October 2017

Published online:

13 November 2017

© Springer Science+Business Media, LLC 2017

## ABSTRACT

The solid/liquid interfacial energies of pure metals and metallic alloys are modelled in this paper. A simple model is offered for pure metals, showing that their solid/liquid interfacial energy ( $\sigma$ ) slightly increases with temperature.  $\sigma$  for metallic alloys is considered for the interface between solid and liquid solutions being in thermodynamic equilibrium, calculated by the CALPHAD method. The Butler equation is extended to find the equilibrium composition of the solid/liquid interfacial region and the solid/liquid interfacial energy at fixed temperatures. This method takes into account the segregation of low-interfacial energy components to the solid/liquid interfacial region. It is shown how the new method can be extended to multi-component alloys. The method is applied to calculate the solid/liquid interfacial energy of Al-rich solid solutions in equilibrium with eutectic liquid alloys of Al–Cu, Al–Ni, Al–Ag and Al–Ag–Cu systems. Good agreement was found with experimental values. For the Al–Ag–Cu system, the modelled value allows to select the more probable experimental value from the two contradicting experimental values published in the literature. The solid/liquid interfacial energy is calculated for the eutectic Ag–Cu system as function of liquidus composition (which determines both the equilibrium solidus composition and the equilibrium temperature). Finally it is claimed that using solely bulk thermodynamic data (melting enthalpy and molar volumes of pure components and molar excess Gibbs energies of equilibrium solid and liquid solutions) it is possible to provide meaningful values for the temperature and concentration dependence of solid/liquid interfacial energies of alloys. The method can be applied for simulation of solid/liquid phase transformation and also to solid/liquid equilibrium calculations of nano-alloys.

After this paper was accepted, the following relevant paper was electronically published: C.Zhang, Y.Du: A novel thermodynamic model for obtaining solid–liquid interfacial energies. Metall Mater Trans A (2017), DOI <https://doi.org/10.1007/s11661-017-4365-6>.

Address correspondence to E-mail: [kaptay@hotmail.com](mailto:kaptay@hotmail.com)

<https://doi.org/10.1007/s10853-017-1778-y>

## Introduction

Solid/liquid interfacial energy ( $\sigma$ ) of alloys [1–3] is an important thermodynamic property needed to model both nucleation [4–9] and grain growth, i.e. the evolution of the microstructure of alloys [10–21]. The same quantity is essential in producing nano-structured materials [22–24], to calculate solid/liquid equilibrium phase diagrams for nano-systems [25–39] or even to predict dissolution kinetics [40]. Since the pioneering experimental work of Turnbull and Cech [41] measurement techniques and interpretation theories have been constantly developed [42–55], it is still a challenge to measure solid/liquid interfacial energy of alloys of any composition [56–63]. As a consequence, the development of a reliable thermodynamic method is needed. Although there are quite a number of methods developed to model  $\sigma$  for one-component metals [64–85] and for alloys [86–92], including the ab initio methods [93–98], segregation is taken into account only in some of them [87, 89].

The goal of this paper is to develop a new model for the solid–liquid interfacial energy of alloys taking into account segregation and to check its validity against experimental values. The present paper is an extension of the method developed by the present author earlier for liquid/liquid and for solid/solid coherent interfacial energies [99], being itself an extension of the Butler equation [100]. The Butler equation (originally designed [100] and applied [101–108] for liquid surfaces) has been recently rederived [109, 110] and applied to different other interfaces [111–113]. The present model is similar to the previous models [87, 89], but it is worked out here in more details.

## The general framework of the model

Let us consider a binary A–B system at standard pressure of 1 bar and at a temperature  $T$  (K) in a two-phase region when a solid solution of composition  $x_{B,S}$  keeps equilibrium with a liquid solution of composition  $x_{B,L}$ , where  $x_{B,S}$  and  $x_{B,L}$  (both dimensionless) are the mole fractions of component B in the solid solution (subscript “S”) and in the liquid solution (subscript “L”), respectively, with the solid and liquid phases separated by a macroscopic planar (and not curved) solid/liquid interface. The goal in the present paper is to develop a method to calculate the

concentration and temperature dependence of the solid/liquid interfacial energy.

In the simplest case of the phase diagram type shown in Fig. 1a, temperature will define both equilibrium values  $x_{B,S}$  and  $x_{B,L}$ . Then, whatever is the average composition of the alloy in the range between  $x_{B,S}$  and  $x_{B,L}$ , the solid/liquid interfacial energy will have a constant value at given temperature, as shown in Fig. 1b. Outside this concentration range, the solid/liquid interfacial energy is not defined. The goal of the present paper is to work out an equation for the T dependence of the solid/liquid interfacial energy as shown in Fig. 1b.

## The equilibrium between the bulk phases

The equilibrium compositions of the phases ( $x_{B,S}$  and  $x_{B,L}$ ) follow from the condition of heterogeneous equilibrium:

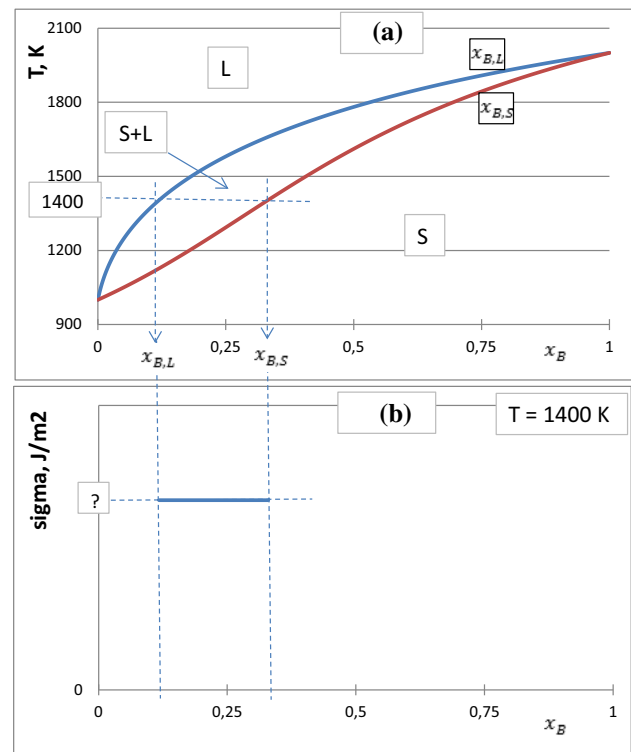


**Figure 1** A simple phase diagram with a two-phase solid–liquid region (a) and the corresponding concentration independence of the solid/liquid interfacial energy at a fixed  $T = 1400$  K (b). **a** is calculated by Eq. (1c–f) using parameters:  $\mu_{A,L}^0 - \mu_{A,S}^0 = 8 \cdot (1000 - T)$ ,  $\mu_{B,L}^0 - \mu_{B,S}^0 = 20 \cdot (2000 - T)$ .

$$\mu_{i,S} = \mu_{i,L} \tag{1}$$

where  $\mu_{i,S}$  (J/mol) is the chemical potential of component  $i$  in the solid solution, while  $\mu_{i,L}$  (J/mol) is the same in the liquid solution. For a binary A–B system described by the regular solution model, the following two equations should be solved simultaneously for  $x_{B,S}$  and  $x_{B,L}$  at given  $T$  and other fixed parameters:

$$\begin{aligned} \mu_{A,S}^{\circ} + R \cdot T \cdot \ln(1 - x_{B,S}) + L_{0,S} \cdot x_{B,S}^2 \\ = \mu_{A,L}^{\circ} + R \cdot T \cdot \ln(1 - x_{B,L}) + L_{0,L} \cdot x_{B,L}^2 \end{aligned} \tag{1a}$$

$$\begin{aligned} \mu_{B,S}^{\circ} + R \cdot T \cdot \ln x_{B,S} + L_{0,S} \cdot (1 - x_{B,S})^2 \\ = \mu_{B,L}^{\circ} + R \cdot T \cdot \ln x_{B,L} + L_{0,L} \cdot (1 - x_{B,L})^2 \end{aligned} \tag{1b}$$

where  $\mu_{A,S}^{\circ}$  (J/mol) is the standard chemical potential of a pure component A in the solid state,  $\mu_{A,L}^{\circ}$  (J/mol) is the same in the liquid state,  $\mu_{B,S}^{\circ}$  and  $\mu_{B,L}^{\circ}$  (J/mol) are the same for component B,  $R = 8.3145$  J/molK is the universal gas constant,  $T$  (K) is the absolute temperature,  $L_{0,L}$  (J/mol) is the zeroth-order interaction energy for the liquid solution in the Redlich–Kister formalism, being the same as the interaction energy in the regular solution model and  $L_{0,S}$  (J/mol) is the same for the solid solution. Equation (1a, b) has the following simple analytical solution for the ideal solutions ( $L_{0,L} = L_{0,S} = 0$ ):

$$x_{B,L} = \frac{K_A - 1}{K_A - K_B} \tag{1c}$$

$$x_{B,S} = K_B \cdot x_{B,L} \tag{1d}$$

$$K_A \equiv \exp\left(\frac{\mu_{A,L}^{\circ} - \mu_{A,S}^{\circ}}{R \cdot T}\right) \tag{1e}$$

$$K_B \equiv \exp\left(\frac{\mu_{B,L}^{\circ} - \mu_{B,S}^{\circ}}{R \cdot T}\right) \tag{1f}$$

Figure 1a is drawn by Eq. (1c–f) using parameters:  $\mu_{A,L}^{\circ} - \mu_{A,S}^{\circ} = 8 \cdot (1000 - T)$  and  $\mu_{B,L}^{\circ} - \mu_{B,S}^{\circ} = 20 \cdot (2000 - T)$ , as an example.

### The equilibrium at the solid/liquid interface

In Fig. 2, a system containing a bulk solid solution and a bulk liquid solution with an interface between them is shown schematically. The width of the interface is not defined in this paper. It is only defined that it has a special equilibrium mole fraction of component B, denoted as  $x_{B,S/L}$ , being generally different from both  $x_{B,S}$  and  $x_{B,L}$ .

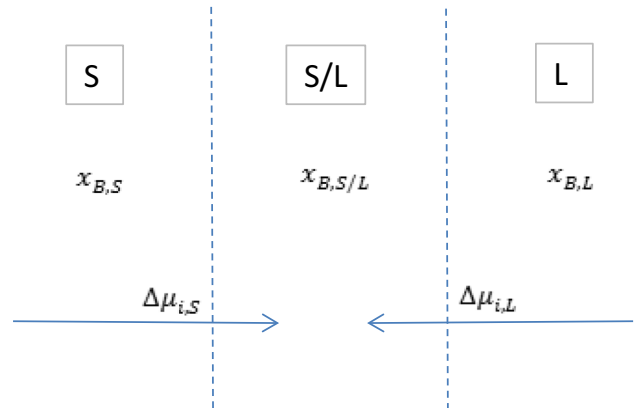


**Figure 2** Schematic of the solid and liquid bulk phases with the interface between them.

According to the general model of the partial interfacial energy of a component, it is calculated as the change of the chemical potential of the given component accompanying the transport of the same component from the bulk phase to the interfacial region divided by the molar interfacial area of the same component [100, 109]. In case of two condensed phases surrounding the given interface, the average value calculated from the two bulk phases is taken as [109]:

$$\sigma_i = \frac{\Delta\mu_{i,S} + \Delta\mu_{i,L}}{2 \cdot \omega_i} \tag{2}$$

where  $\sigma_i$  (J/m<sup>2</sup>) is the partial solid/liquid interfacial energy of component  $i$  ( $i = A$  or  $B$  in the binary A–B system),  $\Delta\mu_{i,S}$  (J/mol) is the change of the chemical potential of component  $i$  accompanying the transport of this component from the bulk solid phase to the interfacial region,  $\Delta\mu_{i,L}$  (J/mol) is the change of the chemical potential of component  $i$  accompanying the transport of this component from the bulk liquid phase to the interfacial region and  $\omega_i$  (m<sup>2</sup>/mol) is the molar interfacial area of component  $i$ . The two chemical potential changes are defined as:

$$\Delta\mu_{i,S} \equiv \mu_{i,S/L} - \mu_{i,S} \tag{2a}$$

$$\Delta\mu_{i,L} \equiv \mu_{i,S/L} - \mu_{i,L} \tag{2b}$$

where  $\mu_{i,S/L}$  (J/mol) is the chemical potential of component  $i$  in the S/L interfacial region,  $\mu_{i,S}$  (J/mol) is the same in the bulk of the solid phase and  $\mu_{i,L}$  (J/mol) is the same in the bulk of the liquid phase. Substituting Eq. (2a, b) into Eq. (2):

$$\sigma_i = \frac{2 \cdot \mu_{i,S/L} - \mu_{i,S} - \mu_{i,L}}{2 \cdot \omega_i} \quad (3)$$

The chemical potentials in the two bulk phases are written by the following usual expressions:

$$\mu_{i,S} = \mu_{i,S}^o + R \cdot T \cdot \ln x_{i,S} + \Delta G_{i,S}^E \quad (4a)$$

$$\mu_{i,L} = \mu_{i,L}^o + R \cdot T \cdot \ln x_{i,L} + \Delta G_{i,L}^E \quad (4b)$$

where  $\Delta G_{i,S}^E$  (J/mol) is the partial molar excess Gibbs energy of component  $i$  in the solid solution and  $\Delta G_{i,L}^E$  (J/mol) is the same in the liquid solution. The chemical potential of the component in the  $S/L$  interfacial region is written by a similar equation:

$$\mu_{i,S/L} = \mu_{i,S/L}^o + R \cdot T \cdot \ln x_{i,S/L} + \Delta G_{i,S/L}^E \quad (4c)$$

where  $\mu_{i,S/L}^o$  (J/mol) is the standard chemical potential of the pure component  $i$  in the solid/liquid interfacial region,  $x_{i,S/L}$  (dimensionless) is the mole fraction of component  $i$  in the solid/liquid interfacial region and  $\Delta G_{i,S/L}^E$  (J/mol) is the partial excess Gibbs energy of component  $i$  in the solid/liquid interfacial region. Substituting Eq. (4a–c) into Eq. (3), after some rearrangements:

$$\sigma_i = \sigma_i^o + \frac{R \cdot T}{\omega_i} \cdot \ln \left( \frac{x_{i,S/L}}{\sqrt{x_{i,S} \cdot x_{i,L}}} \right) + \frac{2 \cdot \Delta G_{i,S/L}^E - \Delta G_{i,S}^E - \Delta G_{i,L}^E}{2 \cdot \omega_i} \quad (5)$$

where  $\sigma_i^o$  (J/m<sup>2</sup>) is the solid/liquid interfacial energy of the pure component  $i$ , defined as:

$$\sigma_i^o \equiv \frac{2 \cdot \mu_{i,S/L}^o - \mu_{i,S}^o - \mu_{i,L}^o}{2 \cdot \omega_i} \quad (6)$$

The  $\sigma_i^o$  and  $\omega_i$  values are temperature dependent. In the best-case scenario, they are known for each pure substance, or they can be found by modelling. For the two-component A–B system, the mole fraction of component B is written as  $x_B$ , while that of component A is written as  $(1 - x_B)$ . Substituting these values into Eq. (5), the partial solid/liquid interfacial energies of components A and B are obtained as:

$$\sigma_A = \sigma_A^o + \frac{R \cdot T}{\omega_A} \cdot \ln \left( \frac{1 - x_{B,S/L}}{\sqrt{(1 - x_{B,S}) \cdot (1 - x_{B,L})}} \right) + \frac{2 \cdot \Delta G_{A,S/L}^E - \Delta G_{A,S}^E - \Delta G_{A,L}^E}{2 \cdot \omega_A} \quad (7a)$$

$$\sigma_B = \sigma_B^o + \frac{R \cdot T}{\omega_B} \cdot \ln \left( \frac{x_{B,S/L}}{\sqrt{x_{B,S} \cdot x_{B,L}}} \right) + \frac{2 \cdot \Delta G_{B,S/L}^E - \Delta G_{B,S}^E - \Delta G_{B,L}^E}{2 \cdot \omega_B} \quad (7b)$$

The bulk equilibrium mole fractions  $x_{B,S}$  and  $x_{B,L}$  follow from bulk equilibrium of the solid and liquid phases and can be read from the phase diagram at given temperature as shown in Fig. 1a and Eq. 1c–f. The equilibrium mole fraction in the interfacial region  $x_{B,S/L}$  can be found by extending the Butler equation for the solid/liquid interface [100, 109, 110]:

$$\sigma = \sigma_A = \sigma_B \quad (8)$$

Substituting Eq. (7a, b) into the right-hand side of Eq. (8), the equilibrium value of  $x_{B,S/L}$  can be found. Substituting this value back into any of Eq. (7a, b), the solid/liquid interfacial energy is obtained, in agreement with Eq. (8). To perform this calculation, the excess partial Gibbs energies are usually described by the Redlich–Kister polynomials, using different interaction energies for solid and liquid solutions obtained from a CALPHAD assessment for the given system.

### The application of the present model to ideal solutions

Equations (7, 8) have analytical solution only if both solid and liquid solutions are taken as ideal ( $L_{0,S} = L_{0,L} = 0$ ) and if the atomic sizes and interfacial arrangements of the two components are equal ( $\omega_A = \omega_B = \omega$ ). In this case, Eq. (7a, b) are rewritten as:

$$\sigma_A = \sigma_A^o + \frac{R \cdot T}{\omega} \cdot \ln \left( \frac{1 - x_{B,S/L}}{\sqrt{(1 - x_{B,S}) \cdot (1 - x_{B,L})}} \right) \quad (9a)$$

$$\sigma_B = \sigma_B^o + \frac{R \cdot T}{\omega} \cdot \ln \left( \frac{x_{B,S/L}}{\sqrt{x_{B,S} \cdot x_{B,L}}} \right) \quad (9b)$$

Substituting these equations into the Butler equation Eq. (8) ( $\sigma_A = \sigma_B$ ), the following equation is obtained for  $x_{B,S/L}$ :

$$x_{B,S/L} = \frac{K_{B,seg}}{K_{B,seg} + \sqrt{\frac{(1-x_{B,S}) \cdot (1-x_{B,L})}{x_{B,S} \cdot x_{B,L}}}} \quad (9c)$$

where  $K_{B,seg}$  (dimensionless) is the segregation coefficient of component B, defined as:

$$K_{B,seg} \equiv \exp \left[ \frac{\omega \cdot (\sigma_A^o - \sigma_B^o)}{R \cdot T} \right] \tag{9d}$$

Now, let us apply Eqs. (1c–f, 9c, d) to calculate  $x_{B,L}$ ,  $x_{B,S}$  and  $x_{B,S/L}$  as function of  $T$  for the following model parameters, as an example:  $\mu_{A,L}^o - \mu_{A,S}^o = 8 \cdot (1000 - T)$ ,  $\mu_{B,L}^o - \mu_{B,S}^o = 20 \cdot (2000 - T)$ ,  $\sigma_A^o = 0.15 \text{ J/m}^2$ ,  $\sigma_B^o = 0.30 \text{ J/m}^2$ ,  $\omega = 40,000 \text{ m}^2/\text{mol}$ . The results of calculations for  $x_{B,S/L}$  are shown in Fig. 3. Substituting the values of  $x_{B,S/L}$  found by Eq. (9c, d) into Eqs. (8, 9a, b), the solid/liquid interfacial energy of the alloy is calculated. Repeating the same procedure at different temperatures, the temperature dependence of the interfacial energy is found as shown in Fig. 4. A negative deviation from the additive rule in Fig. 4 is found despite the fact that an ideal solution is considered. It is obviously due to the segregation of component A to the interface. This is because component A is interface-active as it has a lower solid/liquid interfacial energy for its pure state compared to component B. For the same reason, the dotted line corresponding to the composition of the solid/liquid interfacial region deviates from the additive rule towards alloys with higher A content in Fig. 3. This effect of segregation makes our present new method superior compared to previous published models. Let us note that increasing the value of  $K_{B,seg}$  the dotted line in Fig. 3 shifts from the left top corner towards the right bottom corner of the diagram.

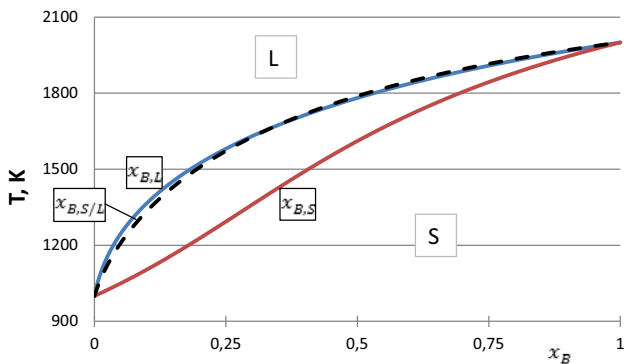


**Figure 3** Same as Fig. 1a, but with the concentration values of  $x_{B,S/L}$  shown by the dotted line. Calculations by Eqs. (1c–f, 9a, c, d) with parameters:  $\mu_{A,L}^o - \mu_{A,S}^o = 8 \cdot (1000 - T)$ ,  $\mu_{B,L}^o - \mu_{B,S}^o = 20 \cdot (2000 - T)$ ,  $\sigma_A^o = 0.15 \text{ J/m}^2$ ,  $\sigma_B^o = 0.30 \text{ J/m}^2$ ,  $\omega = 40,000 \text{ m}^2/\text{mol}$ .

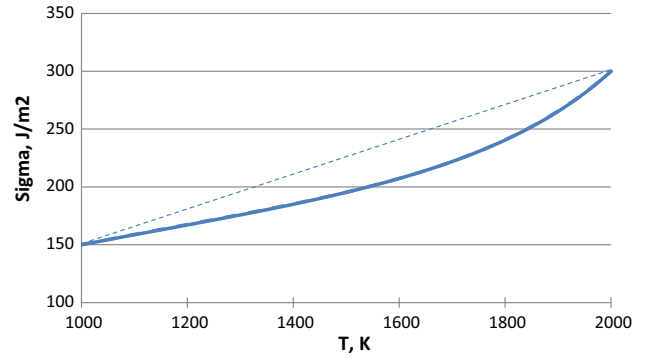


**Figure 4** Temperature dependence of the solid/liquid interfacial energy for the case of Figs. 1a, 3. The bold line is calculated by Eqs. (8, 9a, b) using parameters of Fig. 3. The straight dotted line shows the additive rule to help the eye.

### On the interaction energies in the solid/liquid interfacial region

The interaction energy in the solid/liquid interfacial region in the first estimation can be calculated as the average of the interaction energies in the liquid phase and in the solid phase:

$$L_{j,S/L} \cong 0.5 \cdot (L_{j,L} + L_{j,S}) \tag{10}$$

where  $L_{j,S/L}$  (J/mol) is the  $j$ th interaction energy of the components in the solid/liquid interfacial region,  $L_{j,L}$  (J/mol) is the same in the bulk liquid solution and  $L_{j,S}$  (J/mol) is the same in the bulk solid solution. Equations (7–8, 10) are the central equations of our new model to estimate the concentration and temperature dependence of solid/liquid interfacial energy of alloys. As an example, in the framework of the regular solution model, when only the zeroth-order interaction energies are used, Eq. (7a, b) can be rewritten using Eq. (10) as:

$$\sigma_A = \sigma_A^o + \frac{R \cdot T}{\omega_A} \cdot \ln \left( \frac{1 - x_{B,S/L}}{\sqrt{(1 - x_{B,S}) \cdot (1 - x_{B,L})}} \right) + \frac{L_{0,L} \cdot (x_{B,S/L}^2 - x_{B,L}^2) + L_{0,S} \cdot (x_{B,S/L}^2 - x_{B,S}^2)}{2 \cdot \omega_A} \tag{10a}$$

$$\sigma_B = \sigma_B^o + \frac{R \cdot T}{\omega_B} \cdot \ln \left( \frac{x_{B,S/L}}{\sqrt{x_{B,S} \cdot x_{B,L}}} \right) + \frac{L_{0,L} \cdot [(1 - x_{B,S/L})^2 - (1 - x_{B,L})^2] + L_{0,S} \cdot [(1 - x_{B,S/L})^2 - (1 - x_{B,S})^2]}{2 \cdot \omega_B} \tag{10b}$$



Looking at Eq. (10a, b) it is more obvious how  $x_{B,S/L}$  can be found by substituting Eq. (10a, b) into Eq. (8) ( $\sigma_A = \sigma_B$ ) at a given set of state parameters ( $T, x_{B,S}, x_{B,L}$ ), if the following parameters are known:  $\sigma_A^o, \sigma_B^o, \omega_A, \omega_B, L_{0,S}, L_{0,L}$ . Equation (10a, b) are written for the most simple case of the regular solution. Generally Eq. (7a, b) should be used, taking into account Eq. (10) for each interaction energy value.

### Extension of the present model to multi-component alloys

Equations (7a, b, 8) can be extended to ternary A–B–C alloys, as well, taking also into account the materials balance equations:

$$\sigma_A = \sigma_A^o + \frac{R \cdot T}{\omega_A} \cdot \ln \left( \frac{x_{A,S/L}}{\sqrt{x_{A,S} \cdot x_{A,L}}} \right) + \frac{2 \cdot \Delta G_{A,S/L}^E - \Delta G_{A,S}^E - \Delta G_{A,L}^E}{2 \cdot \omega_A} \quad (11a)$$

$$\sigma_B = \sigma_B^o + \frac{R \cdot T}{\omega_B} \cdot \ln \left( \frac{x_{B,S/L}}{\sqrt{x_{B,S} \cdot x_{B,L}}} \right) + \frac{2 \cdot \Delta G_{B,S/L}^E - \Delta G_{B,S}^E - \Delta G_{B,L}^E}{2 \cdot \omega_B} \quad (11b)$$

$$\sigma_C = \sigma_C^o + \frac{R \cdot T}{\omega_C} \cdot \ln \left( \frac{x_{C,S/L}}{\sqrt{x_{C,S} \cdot x_{C,L}}} \right) + \frac{2 \cdot \Delta G_{C,S/L}^E - \Delta G_{C,S}^E - \Delta G_{C,L}^E}{2 \cdot \omega_C} \quad (11c)$$

$$\sigma = \sigma_A = \sigma_B = \sigma_C \quad (11d)$$

$$x_{A,S} + x_{B,S} + x_{C,S} = 1 \quad (11e)$$

$$x_{A,L} + x_{B,L} + x_{C,L} = 1 \quad (11f)$$

$$x_{A,S/L} + x_{B,S/L} + x_{C,S/L} = 1 \quad (11g)$$

First, the equilibrium compositions of the bulk solid ( $x_{i,S}$ ) and bulk liquid ( $x_{i,L}$ ) phases are calculated by the CALPHAD method. The equilibrium composition of the solid/liquid interface ( $x_{i,S/L}$ ) is calculated by substituting Eq. (11a–c) into different parts of Eq. (11d) ( $\sigma_A = \sigma_B$  and  $\sigma_A = \sigma_C$ ), taking into account also the materials balance Eqs. (10) and (11g). The equilibrium composition of the interface can be substituted back into Eq. (11a–c) to find the partial solid/liquid interfacial energies, which should be identical within the uncertainty of the numerical method. Their average value provides the requested value for the solid/liquid interfacial energy of the given alloy, in accordance with Eq. (11d).

The same method can be logically extended to higher-order systems, extending further Eqs. (7a, b, 8, 10) for the binary systems and Eqs. (10, 11a–g) for the ternary systems.

### The model for pure metals

As follows from the above, the temperature dependences of the solid/liquid interfacial energies and molar interfacial areas of the pure components are needed to model the solid/liquid interfacial energy of multi-component alloys. As these data are usually not available, simple models will be offered herewith. The goal is to connect these missing complex quantities with the simplest and well-known thermodynamic properties, such as melting enthalpy and molar volume of the pure metals.

The present model on interfacial energies will be built using the general definition of Eq. (6) for the solid/liquid interfacial energy of pure components. The two differences in chemical potentials of Eq. (6) are written through the enthalpy and entropy terms as:

$$\mu_{i,S/L}^o - \mu_{i,S}^o = (H_{i,S/L}^o - H_{i,S}^o) - T \cdot (S_{i,S/L}^o - S_{i,S}^o) \quad (12a)$$

$$\mu_{i,S/L}^o - \mu_{i,L}^o = (H_{i,S/L}^o - H_{i,L}^o) - T \cdot (S_{i,S/L}^o - S_{i,L}^o) \quad (12b)$$

where  $H_{i,S/L}^o$  (J/mol) is the standard enthalpy of pure component  $i$  in the solid/liquid interface region,  $H_{i,S}^o$  (J/mol) is the same in the bulk solid phase,  $H_{i,L}^o$  (J/mol) is the same in the bulk liquid phase,  $S_{i,S/L}^o$  (J/molK) is the standard entropy of pure component  $i$  in the solid/liquid interface region,  $S_{i,S}^o$  (J/molK) is the same in the bulk solid phase and  $S_{i,L}^o$  (J/molK) is the same in the bulk liquid phase.

The enthalpy and entropy differences of Eq. (12a, b) are estimated supposing that the solid/liquid region is liquid-like, adsorbed to the outer plane of the solid crystal. Because of this, the atoms within the crystal have approximately the same freedom as the atoms in its surface, i.e. the entropies of atoms within a crystal and in its surface region are approximately the same:

$$(S_{i,S/L}^o - S_{i,S}^o) \cong 0 \quad (13a)$$

On the other hand, the atoms within bulk liquid have more freedom to move around compared to the adsorbed liquid atoms along its interface with the solid crystal. Thus, the liquid atoms in the interfacial region lose half of their configurational freedom characteristic for the bulk liquid, leading to the following approximated equation:

$(S_{i,S/L}^o - S_{i,L}^o) \cong -\frac{1}{2} \cdot \Delta_m S_{conf}^o$ , where  $\Delta_m S_{conf}^o$  is the configurational part of the melting entropy of a general pure metal. The latter can be approximated as [114]:  $\Delta_m S_{conf}^o \cong R \cdot \ln 2$ . (Note that the same expression is valid for the configurational entropy of the equimolar binary solution, but it is just a coincidence.) Substituting this expression into the previous one, the final equation is obtained as:

$$(S_{i,S/L}^o - S_{i,L}^o) \cong -0.5 \cdot R \cdot \ln 2 = -2.88 \text{ J/molK} \quad (13b)$$

As the solid/liquid interface is liquid-like, there is almost no cohesion energy change from the liquid side; thus, the following equation is approximately valid:

$$(H_{i,S/L}^o - H_{i,L}^o) \cong 0 \quad (13c)$$

On the other hand, the cohesion energy within the solid crystal is decreased by the standard melting enthalpy when the atom is transferred from the bulk of the crystal into the liquid-like interfacial region, i.e.:

$$(H_{i,S/L}^o - H_{i,S}^o) \cong \Delta_m H_i^o \quad (13d)$$

where  $\Delta_m H_i^o$  (J/mol) is the standard molar enthalpy of melting of a pure component *i*.

The molar interfacial area of component *i* is calculated as [115]:

$$\omega_i = f \cdot V_i^{2/3} \cdot N_{Av}^{1/3} \quad (14a)$$

$$f = \left(\frac{3 \cdot f_b}{4}\right)^{2/3} \cdot \frac{\pi^{1/3}}{f_i} \quad (14b)$$

where  $V_i$  (m<sup>3</sup>/mole) is the characteristic molar volume of the pure component *i* at the solid/liquid interface at given temperature,  $N_{Av} = 6.02 \times 10^{23} \text{ mol}^{-1}$  is the Avogadro number and *f* (dimensionless) is a structural parameter depending on the packing ratios of the bulk phases ( $f_b$ ) and that of the interface ( $f_i$ ). As follows from the above, the solid/liquid interfacial region is liquid-like. Therefore, the molar volume in Eq. (14a) is taken as the molar volume of

the pure liquid metal and  $f_b$  (the bulk packing fraction) in Eq. (14a) is also taken as the bulk packing fraction of the liquid metal. As was shown in [115], the average value for simple liquid metals (resulting from bcc, fcc and hcp metals) is:  $f_b \cong 0.65 \pm 0.02$ , being also consistent with the bulk random packing fraction of equal spheres [116, 117]. On the other hand,  $f_i$  (the packing fraction in the solid/liquid interface) is taken as the packing fraction of the outer crystal plane of the solid crystal, as the liquid is adsorbed to it. For the most dense crystal plane (such as the 111 plane of the fcc crystal),  $f_i = 0.906$  [115]. Substituting these two latter values into Eq. (14b),  $f \cong 1.00$ . Let us note that anisotropy of interfacial energy is neglected in this paper for simplicity, as it has a small magnitude [118].

In this model, the excess molar volumes of both the solid and liquid solutions are neglected for simplicity, that is why the molar interfacial areas of the components are taken as independent of the composition, and thus, they are taken equal in both Eqs. (5, 6).

The temperature dependence of the molar volumes of fcc metals is known in the liquid state using the following semi-empirical equations [119]:

$$V_i = a + b \cdot T^n \quad \text{below the melting point} \quad (15a)$$

$$V_i = c + d \cdot T \quad \text{above the melting point} \quad (15b)$$

with semi-empirical parameters *a*, *b*, *n*, *c*, *d* given in Table 1 for fcc metals. Substituting Eq. (13a–d) into Eq. (12a, b) and substituting the resulting equation and Eqs. (14a, 15a–b) with  $f \cong 1.00$  into Eq. (6), the following final equations are obtained:

$$\sigma_i^o \cong \frac{\Delta_m H_i^o + 0.5 \cdot R \cdot T \cdot \ln 2}{2 \cdot (a + b \cdot T^n)^{2/3} \cdot N_{Av}^{1/3}} \quad \text{below the melting point} \quad (16a)$$

$$\sigma_i^o \cong \frac{\Delta_m H_i^o + 0.5 \cdot R \cdot T \cdot \ln 2}{2 \cdot (c + d \cdot T)^{2/3} \cdot N_{Av}^{1/3}} \quad \text{above the melting point} \quad (16b)$$

Equation (16a, b) can be generally written as:

$$\sigma_i^o \cong \frac{\alpha \cdot \Delta_m H_i^o + \beta \cdot R \cdot T}{V_i^{2/3} \cdot N_{Av}^{1/3}} \quad (16c)$$

where  $\alpha$  and  $\beta$  (dimensionless) are semi-empirical model parameters. Comparing Eq. (16a, b) with Eq. (16c), the parameter values for our new model are:  $\alpha = 0.5$ ,  $\beta = 0.173$ . The melting enthalpies of

**Table 1** Modelled solid/liquid interfacial energies ( $\pm 10\%$ ) for fcc metals using Eq. (16a, b)

Me	$T_m$ K	$a$ cm <sup>3</sup> /mol	$b^* 10^5$ cm <sup>3</sup> /molK <sup>n</sup>	$n$	$c$ cm <sup>3</sup> /mol	$d^* 10^4$ cm <sup>3</sup> /molK	$\Delta_m H_i^0$ kJ/mol	$\sigma_{i,0K}^0$ mJ/m <sup>2</sup>	$\sigma_{i,T_m}^0$ mJ/m <sup>2</sup>
Ag	1235	10.49	9.646	1.314	10.14	11.85	11.3	140	172
Al	933	10.269	3.860	1.491	9.761	16.54	10.67	134	157
Au	1337	10.396	9.528	1.272	10.15	8.586	12.7	158	195
Cu	1358	7.226	4.06	1.355	6.973	7.123	13.0	206	252
Ir	2719	8.866	1.847	1.377	8.493	5.014	26.4	365	441
Ni	1728	6.718	2.936	1.355	6.464	5.614	17.6	293	351
Pb	600.6	18.21	46.67	1.229	17.93	24.83	5.12	43.8	56.2
Pd	1828	9.047	4.597	1.321	8.746	6.768	17.2	235	287
Pt	2042	9.321	5.120	1.274	9.090	5.265	19.7	263	323
Rh	2237	8.569	1.753	1.414	8.173	6.039	21.55	305	369

\*Melting point and heat of fusion are taken from [120], and parameters a, b, n, c and d are taken from [119]

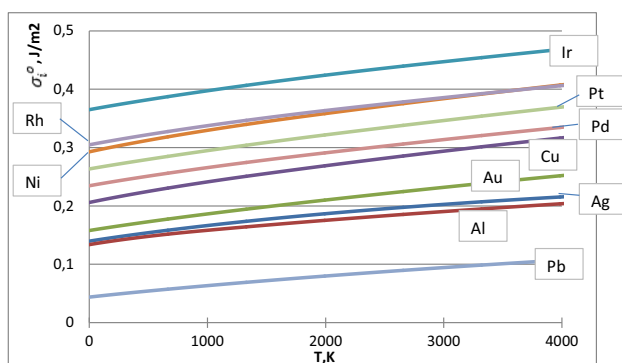


**Figure 5** Modelled solid/liquid interfacial energies of pure fcc metals as function of temperature by Eq. (16a, b) using the data given in Table 1.

metals are taken in the first approximation as T-independent quantities from [120]. The T dependence of the solid/liquid interfacial energies of the 10 fcc metals for 0 K and for the melting points is given in Table 1. The T dependences are shown in Fig. 5, calculated by Eq. (16a, b). All modelled values have an uncertainty of  $\pm 10\%$ .

As follows from Eq. (16a–c), interfacial energy of a metal at a fixed temperature is higher for lower molar volume and higher melting point. The interfacial energy increases with melting point, as the melting entropies are approximately constant (especially for the group of fcc metals considered here), and that is why higher melting points mean higher melting enthalpies. This is in agreement with the original approximation of Turnbull [64, 65]. The interfacial energy values for fcc metals range from 43.8 mJ/m<sup>2</sup> for Pb at  $T = 0$  K to 468 mJ/m<sup>2</sup> for Ir at  $T = 4000$  K.

Thus, more than an order of magnitude change is expected in solid/liquid interfacial energies of fcc alloys as function of composition and temperature. This is especially important for nucleation calculations, as the activation energy of nucleation is proportional to the cube of the interfacial energy. Thus, the activation energy of nucleation can change more than 3 orders of magnitudes for fcc metal-based alloys as function of composition and temperature. This shows the importance of the present model.

### The validation of the method for some fcc eutectic alloys

As in Table 1 only fcc metals are shown, our method to calculate the solid/liquid interfacial energy of alloys will be validated for fcc alloys. For the purpose of validation high-precision, experimental data are needed, found only for the Al-rich eutectics of the Al–Cu, Al–Ni, Al–Ag and Ag–Al–Cu systems. That is why the reliability of the new method will be checked only for these three binary and one ternary system.

#### Trial calculations for binary eutectic Al–Cu, Al–Ni and Ag–Al systems

For the Al–Cu system, the solid/liquid interfacial energy between the Al-rich fcc solid solution and the eutectic liquid solution was measured at the eutectic temperature using the grain boundary groove method and the results were found as  $163.4 \pm 16.2$  mJ/m<sup>2</sup> [49] and  $160.0 \pm 19.2$  mJ/m<sup>2</sup>



[52]. The magnitude of anisotropy in solid/liquid interfacial energy in this system is measured below 1% [118]. For the Al–Ni system, the solid/liquid interfacial energy between the Al-rich fcc solid solution and the eutectic liquid solution was measured at the eutectic temperature using the same method and the result was found as  $171.6 \pm 18 \text{ mJ/m}^2$  [52]. For the Al–Ag system, the solid/liquid interfacial energy between the Al-rich fcc solid solution and the eutectic liquid solution was measured at the eutectic temperature using the same method and the results was found as  $166.32 \pm 21.62 \text{ mJ/m}^2$  [121]. These values are used here to validate our model.

The eutectic temperatures and compositions of the Al-rich alloys are taken from [121] (Table 2). The molar surface areas and solid/liquid interfacial energies of the pure components Ag, Al, Cu and Ni are calculated by Eqs. (14a–16a) and by the parameters of Table 1 for given eutectic temperatures as shown in Table 2. The interaction energies for the Al–Cu, Al–Ni and Ag–Al solid fcc and liquid solutions are given in Tables 3, 4 and 5, based on the CALPHAD assessments [123, 124]. Using these interaction energies, the molar integral and partial excess Gibbs energies are calculated for the given A–B binary system, as:

$$\Delta G^E = x_B \cdot (1 - x_B) \cdot \left[ \begin{matrix} L_0 + L_1 \cdot (1 - 2 \cdot x_B) + L_2 \cdot (1 - 2 \cdot x_B)^2 + \\ L_3 \cdot (1 - 2 \cdot x_B)^3 + L_4 \cdot (1 - 2 \cdot x_B)^4 \end{matrix} \right] \quad (17a)$$

**Table 2** Results of calculations of the solid/liquid interfacial energies between fcc Al-rich solid solutions and the equilibrium liquid solutions of eutectic compositions at the eutectic temperatures in the Al–Cu, Al–Ni and Ag–Al systems

System A–B quantities	Al–Cu	Al–Ni	Ag–Al
$T_{\text{eut}}$ , K	821	916	839
$x_{B,S}$	0.0248	0.002	0.762
$x_{B,L}$	0.171	0.030	0.625
$\sigma$ , mJ/m <sup>2</sup> measured	$163.4 \pm 16.2$ [49] $160.0 \pm 19.2$ [52]	$171.6 \pm 18$ [52]	$166.32 \pm 21.62$ [121]
$\omega_A$ , m <sup>2</sup> /mol, Eqs. (14a, 15a), Table 1	42,080.7	42,462.1	42,172.3
$\omega_B$ , m <sup>2</sup> /mol, Eqs. (14a, 15a), Table 1	32,605.6	30,962.6	42,151.5
$\sigma_A^o$ , mJ/m <sup>2</sup> , Eq. (16a), Table 1	154.9	156.7	162.6
$\sigma_B^o$ , mJ/m <sup>2</sup> , Eq. (16a), Table 1	235.6	326.8	155.2
$x_{B,S/L}$ , Eqs. (7a, b, 8, 10)	0.0676	0.001343	0.8665
$\sigma$ mJ/m <sup>2</sup> , Eqs. (7a, b, 8, 10)	$164.7 \pm 16$	$159.5 \pm 16$	$172.5 \pm 17$
Deviation $\sigma$ , %	+ 0.8 [49]	– 7.0 [52]	+ 3.7 [121]
Numerical/measured	+ 2.9 [52]		

**Table 3** Interaction energies (J/mol) for the fcc and liquid solution phases for the Al–Cu system [123]

$L_j$	fcc	Liquid
$L_0$	– 53520 + 2 T	– 67094 + 8.555 T
$L_1$	38581–2 T	32148–7.118 T
$L_2$	1170	5915–5.889 T
$L_3$	–	– 8175 + 6.049 T

**Table 4** Interaction energies (J/mol) for the fcc and liquid solution phases of the Al–Ni system [124]

$L_j$	fcc	Liquid
$L_0$	– 162407.75 + 16.212965 T	– 207109.28 + 41.31501 T
$L_1$	73417.798–34.914 T	– 10185.79 + 5.8714 T
$L_2$	33471.014–9.837 T	81204.81 – 31.95713 T
$L_3$	– 30758.01 + 10.253T	4365.35–2.51632 T
$L_4$	–	– 22101.64 + 13.16341 T

**Table 5** Interaction energies (J/mol) for the fcc and liquid solution phases of the Ag–Al system [123]

$L_j$	fcc	Liquid
$L_0$	– 7154 – 19.562 T	– 15,022 – 20.538 T
$L_1$	– 16.541–21.694	– 20,456–17.291 T
$L_2$	4274–27.839 T	– 3821–17.169 T
$L_3$	– 8100	7028–12.247 T
$L_4$	–	7661–5.857 T

$$\Delta G_A^E = x_B^2 \cdot \left[ L_0 + L_1 \cdot (3 - 4 \cdot x_B) + L_2 \cdot (5 - 16 \cdot x_B + 12 \cdot x_B^2) + L_3 \cdot (7 - 36 \cdot x_B + 60 \cdot x_B^2 - 32 \cdot x_B^3) + L_4 \cdot (9 - 64 \cdot x_B + 168 \cdot x_B^2 - 192 \cdot x_B^3 + 80 \cdot x_B^4) \right] \quad (17b)$$

$$\Delta G_B^E = (1 - x_B)^2 \cdot \left[ L_0 + L_1 \cdot (1 - 4 \cdot x_B) + L_2 \cdot (1 - 8 \cdot x_B + 12 \cdot x_B^2) + L_3 \cdot (1 - 12 \cdot x_B + 36 \cdot x_B^2 - 32 \cdot x_B^3) + L_4 \cdot (1 - 16 \cdot x_B + 72 \cdot x_B^2 - 128 \cdot x_B^3 + 80 \cdot x_B^4) \right] \quad (17c)$$

The calculation of the solid/liquid interfacial energies is performed by the numerical solution of Eqs. (7a–b, 8, 10). As given in Table 2, the calculated composition of the solid/liquid interfacial region is richer in Al than the average mole fraction of equilibrium bulk solid and liquid solutions. This is because Al has the lowest interfacial energy compared to Ag, Cu and Ni, and so Al segregates preferentially to the interfacial region. As also given in Table 2, the calculated interfacial energy values deviate only by +0.8%/+2.9%/−7.0%/+3.7% from the 4 measured values for the 3 systems, while both measured and modelled values have an uncertainty of at least 10%. This agreement between the measured and modelled values confirms the validity of the present model.

### Trial calculation for the ternary Ag–Al–Cu system

For the Ag–Al–Cu system, the solid/liquid interfacial energy between the Al-rich fcc solid solution and the eutectic liquid solution was measured at the eutectic temperature using the grain boundary groove method and the result was found as:  $67 \pm 15 \text{ mJ/m}^2$  [125] and  $137.40 \pm 16.49 \text{ mJ/m}^2$  [126]. This large difference in experimental values allows us to use our new theoretical method to decide which of the above two contradicting experimental values is closer to reality.

The eutectic temperatures and compositions of the Al-rich alloys are taken from [127] (Table 6). The molar surface areas and solid/liquid interfacial energies of the pure components Ag, Al and Cu are calculated by Eqs. (14a–16a) and by the parameters of Table 1 at the eutectic temperature (Table 6). The interaction energies for binary Al–Cu, Ag–Al, Ag–Cu and for the ternary Ag–Al–Cu systems for solid fcc

**Table 6** Calculation of the solid/liquid interfacial energy between Al-rich fcc solid solution and the equilibrium eutectic liquid Ag–Al–Cu alloy at the eutectic temperature

Quantity, unit	Value
$T_{\text{eu}}$ , K	775.09
$x_{\text{Al,L}}$	0.7156
$x_{\text{Ag,L}}$	0.1657
$x_{\text{Cu,L}}$	0.1187
$x_{\text{Al,S}}$	0.7861
$x_{\text{Ag,S}}$	0.1642
$x_{\text{Cu,S}}$	0.0497
$\sigma$ , mJ/m <sup>2</sup> , measured	$67 \pm 15$ [125]
	$137.40 \pm 16.49$ [126]
$\omega_{\text{Ag}}$ , m <sup>2</sup> /mol, Eqs. (14a, 15a), Table 1	42005.2
$\omega_{\text{Al}}$ , m <sup>2</sup> /mol, Eqs. (14a, 15a), Table 1	41903.3
$\omega_{\text{Cu}}$ , m <sup>2</sup> /mol, Eqs. (14a, 15a), Table 1	32528.0
$\sigma_{\text{Ag}}^o$ , mJ/m <sup>2</sup> , Eq. (16a), Table 1	161.1
$\sigma_{\text{Al}}^o$ , mJ/m <sup>2</sup> , Eq. (16a), Table 1	154.0
$\sigma_{\text{Cu}}^o$ , mJ/m <sup>2</sup> , Eq. (16a), Table 1	234.2
$x_{\text{Al,S/L}}$ , calculated	0.7795
$x_{\text{Ag,S/L}}$ , calculated	0.1655
$x_{\text{Cu,S/L}}$ , calculated	0.0550
$\sigma = \sigma_{\text{Al}} = \sigma_{\text{Ag}} = \sigma_{\text{Cu}}$ , mJ/m <sup>2</sup> , calculated	$160.5 \pm 16$
$\sigma$ deviation, %, calculated/experimental	140% [125]
	16.8% [126]

**Table 7** Interaction energies (J/mol) for the fcc and liquid solution phases of the Ag–Cu system [123]

$L_j$	fcc	Liquid
$L_0$	$34817 - 8.876 T$	$14463 - 1.516 T$
$L_1$	$- 3207 - 0.570 T$	$- 934 + 0.319 T$

**Table 8** Ternary interaction energies (J/mol) for the fcc and liquid solution phases of the Ag–Al–Cu system [127]

$L_j$	fcc	Liquid
$L_{3,\text{Ag}}$	$72,814.0 - 270.0090 T$	$- 133981.8$
$L_{3,\text{Al}}$	$- 7437.2$	$30555.6 - 72.0962 T$
$L_{3,\text{Cu}}$	$- 124167.3$	$- 165118.4 + 78.6913 T$

and liquid solutions are given in Tables 3, 5, 7, 8 based on the CALPHAD assessments [123, 127]. Using these interaction energies, the molar integral and molar partial excess Gibbs energies are calculated for the Ag–Al–Cu system, as:

$$\begin{aligned} \Delta G_{Ag-Al-Cu}^E &= x_{Ag} \cdot x_{Al} \cdot \sum_j L_{j,Ag-Al} \cdot (x_{Ag} - x_{Al})^j \\ &+ x_{Ag} \cdot x_{Cu} \cdot \sum_j L_{j,Ag-Cu} \cdot (x_{Ag} - x_{Cu})^j \\ &+ x_{Al} \cdot x_{Cu} \cdot \sum_j L_{j,Al-Cu} \cdot (x_{Al} - x_{Cu})^j \\ &+ x_{Ag} \cdot x_{Al} \cdot x_{Cu} \cdot (x_{Ag} \cdot L_{3,Ag} + x_{Al} \cdot L_{3,Al} + x_{Cu} \cdot L_{3,Cu}) \end{aligned} \tag{18}$$

$$\Delta G_{Ag}^E = \Delta G_{Ag-Al-Cu}^E + (1 - x_{Ag}) \cdot \left( \frac{d\Delta G_{Ag-Al-Cu}^E}{dx_{Ag}} \right)_{x_{Al}/x_{Cu} \equiv a} \tag{19a}$$

$$x_{Cu} = \frac{1}{1+a} \cdot (1 - x_{Ag}) \tag{19b}$$

$$x_{Al} = \frac{a}{1+a} \cdot (1 - x_{Ag}) \tag{19c}$$

$$\Delta G_{Al}^E = \Delta G_{Ag-Al-Cu}^E + (1 - x_{Al}) \cdot \left( \frac{d\Delta G_{Ag-Al-Cu}^E}{dx_{Al}} \right)_{x_{Ag}/x_{Cu} \equiv b} \tag{20a}$$

$$x_{Cu} = \frac{1}{1+b} \cdot (1 - x_{Al}) \tag{20b}$$

$$x_{Ag} = \frac{b}{1+b} \cdot (1 - x_{Al}) \tag{20c}$$

$$\Delta G_{Cu}^E = \Delta G_{Ag-Al-Cu}^E + (1 - x_{Cu}) \cdot \left( \frac{d\Delta G_{Ag-Al-Cu}^E}{dx_{Cu}} \right)_{x_{Ag}/x_{Al} \equiv c} \tag{21a}$$

$$x_{Al} = \frac{1}{1+c} \cdot (1 - x_{Cu}) \tag{21b}$$

$$x_{Ag} = \frac{c}{1+c} \cdot (1 - x_{Cu}) \tag{21c}$$

The solid/liquid interfacial energies are calculated by solving numerically Eqs. (10, 11a–g). As given in Table 6, the calculated composition of the interfacial region is richer in Al and slightly in Ag, and is poorer in Cu compared to the average compositions in the bulk solid and liquid solutions. This is because Al and Ag have similar and low interfacial energies compared to Cu, so Al and Ag are interfacial active in the system. As also given in Table 6, the calculated interfacial energy value is larger by 16.8% compared to the data of [126], but larger by 140% compared to the data of [125]. Thus, our model calculations confirm that the experimental values of [126] are probably much closer to the reality than those of [125].

Although the deviation between calculated and experimental [126] data is larger than for the binary systems above, the possible experimental and theoretical intervals still overlap: the possible modelled interval of  $160.5 \pm 16 \text{ mJ/m}^2$  overlaps with the experimentally found possible interval of  $137.40 \pm 16.49 \text{ mJ/m}^2$  by [126]. This proves again the validity of our new model.

### Model calculations for a binary alloy as function of composition and temperature

In this chapter, we calculate the concentration/temperature dependence of the composition and energy for the solid/liquid interfacial region for a binary phase diagram. As the Al–Cu, Al–Ni and Al–Ag binary systems considered in Table 2 all contain intermetallic compounds [122] not considered in this paper, the present calculation will be performed for the eutectic Ag–Cu system with no intermetallic compound [122]. Unfortunately no experimental information on interfacial energies exists for this system to compare our calculated values.

There are three, interconnected quantities in an eutectic phase diagram of Fig. 6a: temperature, liquidus temperature and solidus temperature. The liquidus temperature is selected here as the leading parameter. The other two parameters are calculated by the CALPHAD method, using Eqs. (1, 17a–c) and Table 7. The calculated and measured [122] phase diagrams are very close to each other. The molar surface areas and solid/liquid interfacial energies of the pure components Ag and Cu are calculated by Eqs. (14a–16a) and by the parameters of Table 1 as function of temperature. The interaction energies are given in Table 7 using Eq. (17a–c).

The results of calculations are shown in Fig. 6. The broken line in top Fig. 6 shows the mole fraction of Cu in the solid/liquid interfacial region as function of temperature. The values left from the eutectic point correspond to the equilibrium between the Ag-rich solid solution and the liquid solution, while the values right from the eutectic point correspond to the equilibrium between the Cu-rich solid solution and the liquid solution. One can see that the interfacial region is enriched in Ag if compared to the average

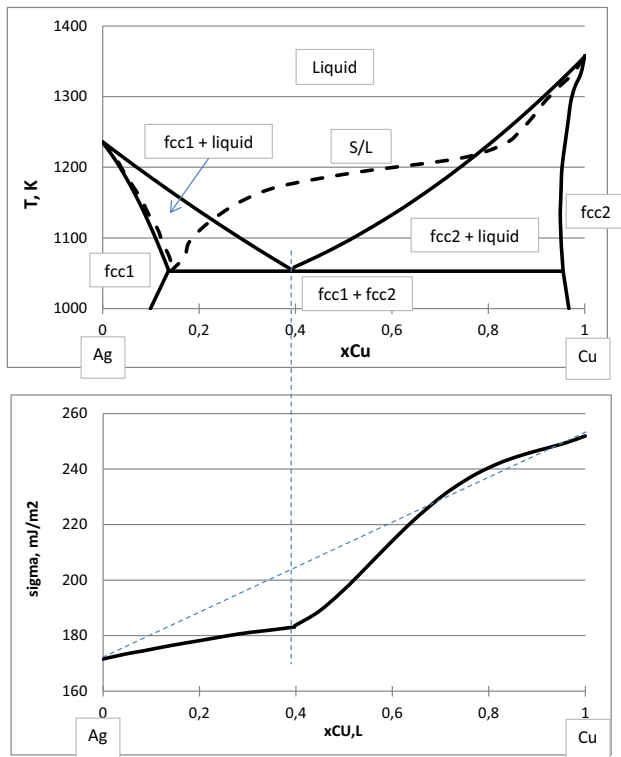


**Figure 6** Equilibrium phase diagram of the Ag–Cu system [122] with the  $T$  dependence of the Cu mole fraction at the solid/liquid interfacial region shown by the dotted line (top figure) and the solid/liquid interfacial energy of the Ag–Cu alloy as function of the liquidus composition with the dotted line showing the additive rule (bottom figure).

solidus and liquidus values at the same temperature. This is because pure Ag has a lower interfacial energy compared to pure Cu, as given in Table 1.

In the bottom part of Fig. 6, the solid/liquid interfacial energy is shown as function of the liquidus mole fraction of Cu. One can see that at the eutectic point the solid/liquid interfacial energies have the same values for Ag-rich and for the Cu-rich solid solutions, keeping equilibrium with the same eutectic liquid. (This is because the partial Gibbs energies of components are identical in these two equilibrium solid solutions.) However, the curve in the bottom part of Fig. 6 is broken in the eutectic point. It also follows from the bottom part of Fig. 6 that the solid/liquid interfacial energy is lower compared to the additive rule shown by a broken straight line. As this seems not be the case for Cu-rich alloys, the same results are shown in Fig. 7 as function of the average solidus and liquidus mole fraction of Cu. As shown in Fig. 7, the modelled values coincide with those calculated by the additive rule in alloys with more

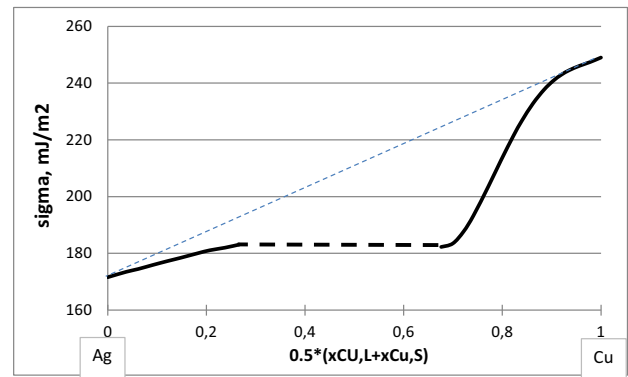


**Figure 7** Solid/liquid interfacial energy of the Ag–Cu alloy as function of the average liquidus and solidus mole fractions of Cu. The horizontal dotted line only shows that at the eutectic point the solid/liquid interfacial energies have the same values when the liquid is in equilibrium with Ag-rich and Cu-rich solid solutions. The thin dotted line shows the additive rule.

than 90 at.% Cu. For all other cases, the modelled values are lower compared to the additive rule. This is explained again by the segregation of Ag to the interfacial region, which follows from the fact that pure Ag has a lower interfacial energy compared to pure Cu (Table 1).

### Discussion on the model parameters of Eq. (16c)

The solid/liquid interfacial energy of pure metals is described by the general Eq. (16c). The above model for pure metals provides the semi-empirical values as:  $\alpha = 0.5$ ,  $\beta = 0.173$ . The calculated results shown in Tables 2 and 6 are obtained using these values. The experimental and modelled values are compared in Fig. 8. As shown in Fig. 8, the correlation coefficient is negative. This is probably due to the not perfectly selected values of parameters  $\alpha$  and  $\beta$ .

All model equations in the literature on solid/liquid interfacial energies of pure metals can be summarized by the general Eq. (6c). However, all literature models provide different values of parameters  $\alpha$  and  $\beta$ . Some models claim  $\alpha = 0$  with some positive value for  $\beta$ , some other models claim  $\beta = 0$  with some positive value of  $\alpha$ , while some models provide both parameters with positive values [64–84]. As follows from the above, our model with  $\alpha = 0.5$ ,  $\beta = 0.173$  is in the interval of possible values, according to the previous models. Based on the

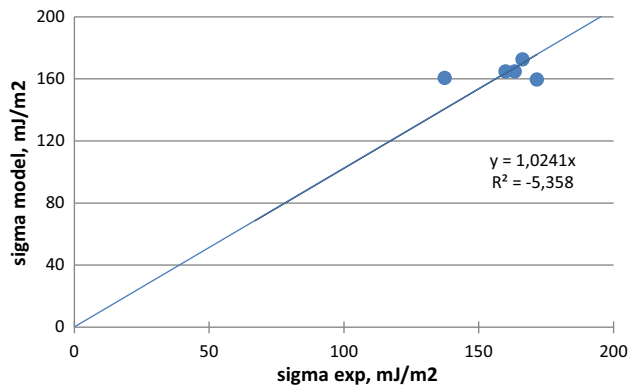


**Figure 8** Comparison of experimental ( $x$ -axis) and modelled ( $y$ -axis) solid/liquid interfacial energies of the 4 eutectic alloys of Tables 2 and 6. The model is based on solid/liquid interfacial energies of pure metals calculated by Eq. (6c) and parameters:  $\alpha = 0.5$ ,  $\beta = 0.173$ .

above, let us check how the two boundary conditions with  $\alpha = 0$  and  $\beta = 0$  perform, optimizing the other nonzero parameter such that the maximum absolute deviation between experimental and modelled values is minimized.

One of the options is shown in Fig. 9 calculated with parameters:  $\alpha = 0.59$ ,  $\beta = 0$ . One can see that the situation in Fig. 9 is not improved compared to Fig. 8. Another option is shown in Fig. 10 calculated with parameters:  $\alpha = 0$ ,  $\beta = 0.925$ . One can see that the situation in Fig. 10 is considerably improved compared to Figs. 8 and 9. In this latter case, all the five experimental data of Table 2 and 6 are within  $\pm 6\%$  of deviation compared to the modelled values, which is the real improvement compared to the 16% of

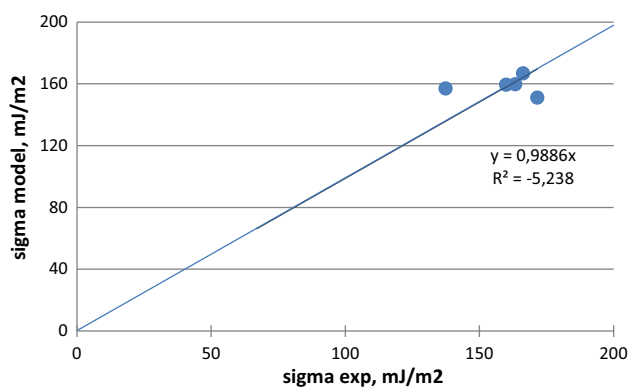


**Figure 9** Comparison of experimental ( $x$ -axis) and modelled ( $y$ -axis) solid/liquid interfacial energies of the 4 eutectic alloys of Tables 2 and 6. The model is based on solid/liquid interfacial energies of pure metals calculated by Eq. (6c) and parameters:  $\alpha = 0.59$ ,  $\beta = 0$ .

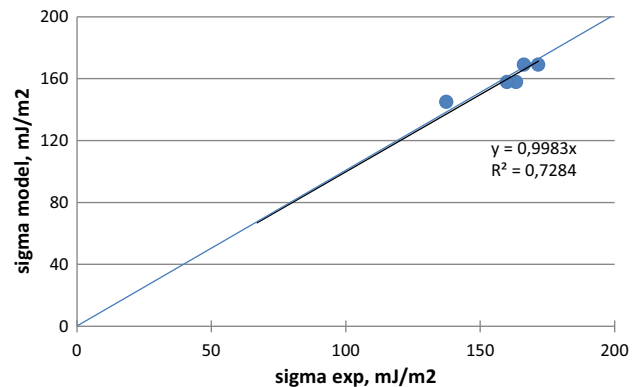


**Figure 10** Comparison of experimental ( $x$ -axis) and modelled ( $y$ -axis) solid/liquid interfacial energies of the 4 eutectic alloys of Tables 2 and 6. The model is based on solid/liquid interfacial energies of pure metals calculated by Eq. (6c) and parameters:  $\alpha = 0$ ,  $\beta = 0.925$ .

difference shown in Table 6. It is clear that if both parameters  $\alpha$  and  $\beta$  are free to optimize, even a better situation can be achieved. However, the five experimental points for the 4 systems are not sufficient to find the generally valid value in this paper. Thus, this topic should be clarified at a later date, based on more numerous and more precise experimental values.

## Conclusions

A general method is developed to model the solid/liquid interfacial energies between an equilibrium solid solution and an equilibrium liquid solution. This new method is the extension of the Butler model developed for liquid/gas surfaces and our previous model developed for liquid/liquid and for coherent solid/solid interfaces. The method allows the calculation of the composition of the interfacial region and its interfacial energy, if the excess Gibbs energies of the neighbouring phases are known as function of composition and temperature. The accuracy of the theoretical method is estimated to be around 10%. The method also takes into account segregation of low-interfacial energy components to the interface, and in this way, the new method is superior to previous models.

For the method to apply, the solid/liquid interfacial energies and the molar interfacial areas of the pure components should be known. Simple models are developed in this paper for the 10 pure fcc metals. Further, the excess molar Gibbs energies of



equilibrium phases should be known, to be taken from CALPHAD assessments.

The present method is validated on the three binary systems: Al–Cu, Al–Ni and Al–Ag. In all three cases, measured values are known for the interface between Al-rich solid solutions and equilibrium eutectic liquids at the eutectic temperature. The agreement between calculated and experimental values is within 7% for each of the 3 binary systems, confirming the validity of the model.

The method is also extended to multi-component systems. It is validated against experimental data on Al–Ag–Cu system, for the interface between Al-rich fcc solid solution and the equilibrium liquid Al–Ag–Cu solution at the eutectic temperature. Among the two existing experimental values, one can be excluded when compared with our calculated values. The agreement between another experiment and our calculated data is acceptable. (The indicated experimental interval overlaps with our calculated interval if 10% of uncertainty is allowed for the model values.) This confirms further the validity of our method. This agreement can be improved if the semi-empirical parameters are fitted to experimental data.

As a final conclusion, we claim that using solely bulk thermodynamic data (melting enthalpy and molar volumes of pure components and molar excess Gibbs energies of equilibrium solid and liquid solutions) it is possible to provide meaningful values for the temperature and concentration dependence of solid/liquid interfacial energies of alloys.

The present method is claimed to be final for the concentration dependence of solid/liquid interfacial energies between solid and liquid solutions of binary and multi-component alloys if the interfacial energies and molar surface areas of the pure metals and the excess Gibbs energies of the solid and liquid bulk alloys are known. However, further work is needed to improve/extend the method to estimate the solid/liquid interfacial energies of pure fcc and/or non-fcc metals as function of temperature. Also, further effort is needed to extend the present method to the interface between intermetallic compounds and liquid alloys.

## Acknowledgements

This work was financed by the GINOP 2.3.2–15–2016–00027 Project. The author is grateful for the

motivating discussion to Liyung Zhang and Yong Du (Central South University, Changsha, China), Stephanie Lippmann (Friedrich Schiller University Jena, Germany), In-Ho Jung (McGill University, Montreal, Canada), Ely Brosh (NRCN, Beer-Sheva, Israel), as well as to Tamas Mende and Andras Dezso (both University of Miskolc, Hungary).

## References

- [1] Jones DRH (1974) Review. The free energies of solid–liquid interfaces. *J Mater Sci* 9:1–17. <https://doi.org/10.1007/BF00554751>
- [2] Eustathopoulos N (1983) Energetics of solid/liquid interfaces of metals and alloys. *Int Met Rev* 28:189–210
- [3] Jones H (2007) An evaluation of measurements of solid/liquid interfacial energies in metallic alloy systems by the groove profile method. *Metall Mater Trans A* 38A:1563–1569
- [4] Zhang L, Stratmann M, Du Y, Sundman D, Steinbach I (2015) Incorporating the CALPHAD sublattice approach of ordering into the phase-field model with finite interface dissipation. *Acta Mater* 88:156–169
- [5] Wang K, Wei M, Zhang L, Du Y (2016) Morphologies of primary silicon in hypereutectic Al–Si alloys: phase-field simulation supported by key experiments. *Metall Mater Trans A* 47A:1510–1516
- [6] Yang J, Hu W (2016) Nucleation and solid–liquid interfacial energy of Li nanoparticles: a molecular dynamics study. *Phys Stat Solidi B* 253:1941–1946
- [7] Lin C, Smith JS, Sinogeikin SV, Kono Y, Park C, Kenney-Benson C, Shen G (2017) A metastable liquid melted from a crystalline solid under decompression. *Nat Commun* 8:14260
- [8] Yoshimura R, Nagaoka S, Nagatomo Y, Esaka H, Shinozuka K (2017) Undercooling for nucleation and volume fraction of primary  $\beta$ -Sn phase in Sn-X alloys. *J Jpn Inst Met Mater* 81:80–88
- [9] Shibuta Y, Sakane S, Miyoshi E, Okita S, Tataka T, Ohno M (2017) Heterogeneity in homogeneous nucleation from billion-atom molecular dynamics simulation of solidification of pure metal. *Nat Commun* 8:10
- [10] Kim WT, Kim SG, Lee JS, Suzuki T (2001) Equilibrium at stationary solid–liquid interface during phase-field modeling of alloy solidification. *Metall Mater Trans A* 32A:961–969
- [11] Choudhury A, Reuther K, Wesner E, August A, Nestler B, Rettenmayr M (2012) Comparison of phase-field and cellular automaton models for dendritic solidification in Al–Cu alloy. *Comput Mater Sci* 55:263–268

- [12] Gubicza J, Hegedűs Z, Lábár JL, Subramanya Sarma V, Kauffmann A, Freudenberger J (2014) Microstructure evolution during annealing of an SPD-processed supersaturated Cu-3at.%Ag alloy. *IOP Conf Ser Mater Sci Eng* 63:012091
- [13] Long J, Zhang W, Wang Y, Du Y, Zhang Z, Lu B, Cheng K, Peng Y (2017) A new type of WC–Co–Ni–Al cemented carbide: grain size and morphology of  $\gamma'$ -strengthened composite binder phase. *Scr Mater* 126:33–36
- [14] Ankit K, Xing H, Selzer M, Nestler B, Glicksman ME (2017) Surface rippling during solidification of binary polycrystalline alloy: insights from 3-D phase-field simulations. *J Cryst Growth* 457:52–59
- [15] Long J, Li K, Chen F, Yi M, Du Y, Lu B, Zhang Z, Wang Y, Cheng K, Zhang K (2017) Microstructure evolution of WC grains in WC–Co–Ni–Al alloys: effect of binder phase composition. *J Alloys Compd* 710:338–348
- [16] Zhang J, Poulsen SO, Gibbs JW, Voorhees PW, Poulsen HF (2017) Determining material parameters using phase-field simulations and experiments. *Acta Mater* 129:229–238
- [17] Kang JL, Xu W, Wei XX, Ferry M, Li JF (2017) Solidification behavior of Co–Sn eutectic alloy with Nb addition. *J Alloys Compd* 695:1498–1504
- [18] Jiang Y, Li D, Liang S, Zou J, Liu F (2017) Phase selection of titanium boride in copper matrix composites during solidification. *J Mater Sci* 52:2957–2963. <https://doi.org/10.1007/s10853-016-0592-2>
- [19] Rodriguez JE, Kreisler C, Volkmann T, Matson DM (2017) Solidification velocity of undercooled Fe–Co alloys. *Acta Mater* 122:431–437
- [20] Yao SW, Liu T, Liu CJ, Yang GJ, Li CX (2017) Epitaxial growth during the rapid solidification of plasma-sprayed molten TiO<sub>2</sub> splat. *Acta Mater* 134:66–80
- [21] Duan SY, Wu CL, Gao Z, Cha LM, Fan TW, Chen JH (2017) Interfacial structure evolution of the growing composite precipitates in Al–Cu–Li alloys. *Acta Mater* 129:352–360
- [22] Wang F, Wu Z, Shanguan X, Sun Y, Feng J, Li Z, Chen L, Zuo S, Zhuo R, Yan P (2017) Preparation of mono-dispersed, high energy release, core/shell structure Al nanopowders and their application in HTPB propellant as combustion enhancers. *Sci Rep* 7:5228
- [23] Sui M, Pandey P, Li MY, Zhang Q, Kunwar S, Lee J (2017) Au-assisted fabrication of nano-holes on c-plane sapphire via thermal treatment guided by Au nanoparticles as catalysts. *Appl Surf Sci* 393:23–39
- [24] Sundaram A, Yang V, Yetter RA (2017) Metal-based nanoenergetic materials: synthesis, properties, and applications. *Progr Energy Combust Sci* 61:293–365
- [25] Kaptay G (2012) Nano-Calphad: extension of the Calphad method to systems with nano-phases and complexions. *J Mater Sci* 47:8320–8335. <https://doi.org/10.1007/s10853-012-6772-9>
- [26] Zhou N, Luo J (2014) Developing thermodynamic stability diagrams for equilibrium-grain-size binary alloys. *Mater Lett* 115:268–271
- [27] Lee J, Sim KJ (2014) General equations of CALPHAD-type thermodynamic description for metallic nanoparticle systems. *Calphad* 44:129–132
- [28] Junkaew A, Ham B, Zhang X, Arróyave R (2014) Tailoring the formation of metastable Mg through interfacial engineering: a phase stability analysis. *Calphad* 45:145–150
- [29] Atanasov I, Ferrando R, Johnston RL (2014) Structure and solid solution properties of Cu–Ag nano alloys. *J Phys: Condens Matter* 26:275301
- [30] Guenther G, Guillon O (2014) Models of size-dependent nanoparticle melting tested on gold. *J Mater Sci* 49:7915–7932. <https://doi.org/10.1007/s10853-014-8544-1>
- [31] Kaptay G, Janczak-Rusch J, Pigozzi G, Jeurgens LPH (2014) Theoretical analysis of melting point depression of pure metals in different initial configurations. *J Mater Eng Perform* 23:1600–1607
- [32] Bajaj S, Haverty MG, Arróyave R, Goddard WA III, Shankar S (2015) Phase stability in nanoscale material systems: extension from bulk phase diagrams. *Nanoscale* 7:9868–9877
- [33] Sopoušek J, Zobač O, Vykoukal V, Buršík J, Roupčová P, Brož P, Pinkas J, Vřešťál J (2015) Temperature stability of AgCu nanoparticles. *J Nanoparticle Res* 17:478
- [34] Minenkov AA, Bogatyrenko SI, Kryshatal AP (2015) Effect of size on eutectic temperature lowering in Ag–Ge layered films. *PSE* 13:383–389
- [35] Zhu J, Fu Q, Xue Y, Cui Z (2016) Comparison of different models of melting transformation of nanoparticles. *J Mater Sci* 51:2262–2269. <https://doi.org/10.1007/s10853-016-9758-1>
- [36] Ferrando R (2016) Theoretical and computational methods for nanoalloy structure and thermodynamics. *Front Nanosci* 10:75–129
- [37] Kaptay G, Janczak-Rusch J, Jeurgens LPH (2016) Melting point depression and fast diffusion in nanostructured brazing fillers confined between barrier nanolayers. *J Mater Eng Perform* 25:3275–3284
- [38] Guisbiers G, Mendoza-Perez R, Bazan-Diaz L, Mendoza-Cruz R, Velazquez-Salazar JJ, Jose-Yacamán M (2017) Size and shape effects on the phase diagrams of nickel-based bimetallic nanoalloys. *J Phys Chem C* 121:6930–6939
- [39] Byrkin VA, Belogorlov AA, Paryohin DA, Mitrofanova AS (2017) Some features of pressure evolution in systems

- “non-wetting liquid/nanoporous medium” at impact intrusion. IOP Conf Ser J Phys Conf Ser 829:012020
- [40] Xiao-Hui W, Ming-Wen C, Zi-Dong W (2016) Analysis of spherical crystal dissolution in the solution. *Acta Phys Sinica* 65:038701
- [41] Turnbull D, Cech RE (1950) microscopic observation of the solidification of small metal droplets. *J Appl Phys* 21:804–810
- [42] Glicksman ME, Vold CL (1969) Determination of absolute solid–liquid interfacial free energies in metals. *Acta Metall* 17:1–11
- [43] Stowell MJ (1970) The solid–liquid interfacial free energy of lead from supercooling data. *Philos Mag* 22:1–6
- [44] Glicksman ME, Vold CL (1971) Establishment of error limits on the solid–liquid interfacial free energy of bismuth. *Ser Metall* 5:493–498
- [45] Nash GE, Glicksman ME (1972) A general method for determining solid–liquid interfacial free energies. *Philos Mag* 25:577–592
- [46] Eustathopoulos N, Coudurier L, Joud JC, Desre P (1976) Tension interfaciale solide-liquide des systemes Al–Sn, Al–In et Al–Sn–In. *J Crystal Growth* 33:105–115
- [47] Passerone A, Sangiorgi R, Eustathopoulos N, Desré P (1979) Microstructure and interfacial tensions in Zn–In and Zn–Bi alloys. *Metal Sci* 13:359–365
- [48] Mondolfo LF, Parisi NL, Kardys J (1984) Interfacial energies on low melting point metals. *Mater Sci Eng* 68:249–266
- [49] Gunduz M, Hunt JD (1985) The measurement of solid–liquid surface energies in the Al–Cu, Al–Si and Pb–Sn systems. *Acta Metall* 33:1651–1672
- [50] Gunduz M, Hunt JD (1989) Solid–liquid surface energy in the Al–Mg system. *Acta Metall* 37:1839–1845
- [51] Cortella L, Vinet B (1995) Undercooling and nucleation studies on pure refractory metals processed in the Grenoble high-drop tube. *Phil Mag* 71:11–21
- [52] Marasli N, Hunt JD (1996) Solid–liquid surface energies in the Al–CuAl<sub>2</sub>, Al–NiAl<sub>3</sub>, and Al–Ti systems. *Acta Metall* 44:1085–1096
- [53] Keslioglu K, Marasli N (2004) Experimental determination of solid–liquid interfacial energy for Zn solid solution in equilibrium with the Zn–Al eutectic liquid. *Metal Mater Trans A* 35A:3665–3672
- [54] Morris JR, Napolitano RE (2004) Developments in determining the anisotropy of solid–liquid interfacial free energy. *JOM* 56:40–44
- [55] Rogers RB, Ackerson BJ (2011) The measurement of solid–liquid interfacial energy in colloidal suspensions using grain boundary grooves. *Phil Mag* 91:682–729
- [56] Paliwal M, Jung IH (2013) Solid/liquid interfacial energy of Mg–Al alloys. *Metall Mater Trans A* 44A(2013):1636–1640
- [57] Kaptay G (2014) A method to estimate interfacial energy between eutectic solid phases from the results of eutectic solidification experiments. *Mater Sci Forum* 790–791:133–139
- [58] Son S, Dong HB (2015) Measuring Solid–liquid interfacial energy by grain boundary groove profile method. *Mater Today Proc* 2:S306–S313
- [59] Mondal S, Phukan M, Ghatak A (2015) Estimation of solid–liquid interfacial tension using curved surface of a soft solid. *Proc Nat Acad Sci USA* 112:12563–12568
- [60] Ozturk E, Aksoz S, Altintas Y, Keslioglu K, Marasli N (2016) Experimental measurements of some thermophysical properties of solid CdSb intermetallic in the Sn–Cd–Sb ternary alloy. *J Thermal Anal Calorimetry* 126:1059–1065
- [61] Maire E, Redston E, Gulda MP, Weitz DA, Spaepen F (2016) Imaging grain boundary grooves in hard-sphere colloidal bicrystals. *Phys Rev E* 94:042604
- [62] Altintas Y, Aksöz S, Keslioglu K, Marasli N (2016) The experimental determination of thermophysical properties of intermetallic CuAl<sub>2</sub> phase in equilibrium with (Al + Cu + Si) liquid. *J Chem Thermod* 97:228–234
- [63] Yoshimura R, Esaka H, Shinozuka K (2017) Influence of Zn addition on the solid/liquid interfacial energy in Sn–Ag alloy. *J Jpn Inst Met Mater* 81:264–269
- [64] Turnbull D (1950) Formation of crystal nuclei in liquid metals. *J Appl Phys* 21:1022–1028
- [65] Turnbull D (1950) Correlation of liquid–solid interfacial energies calculated from supercooling of small droplets. *J Chem Phys* 18:769
- [66] Skapski AS (1956) A next-neighbors theory of maximum undercooling. *Acta Metall* 4:583–585
- [67] Hilliard JE, Cahn JW (1958) On the nature of the interface between a solid metal and its melt. *Acta Metall* 6:772–774
- [68] Miller WA, Chandwick GA (1967) On the magnitude of the solid/liquid interfacial energy of pure metals and its relation to grain boundary melting. *Acta Metall* 15:607–614
- [69] Ewing RH (1971) The free energy of the crystal-melt interface from the radial distribution function. *J Crystal Growth* 11:221–224
- [70] Ewing RH (1972) The free energy of the crystal-melt interface from the radial distribution function -further calculations. *Philos Mag* 25:779–784
- [71] Spaepen F (1975) A structural model for the solid–liquid interface in monatomic systems. *Acta Metall* 23:729–743
- [72] Spaepen F, Meyer RB (1976) The surface tension in a structural model for the solid–liquid interface. *Scripta Metall* 10:257–263

- [73] Waseda Y, Miller WA (1978) Calculation of the crystal–melt interfacial free energy from experimental radial distribution function data. *Trans JIM* 19:546–552
- [74] Miedema AR, den Broeder FJA (1979) On the interfacial energy on solid–liquid and solid–solid metal combinations. *Z Metall* 70:14–20
- [75] Battezzati L (2001) Thermodynamic quantities in nucleation. *Mater Sci Eng, A* 304–306:103–107
- [76] Gránásy L, Tegze M, Ludwig A (1991) Solid–liquid interfacial free energy. *Mater Sci Eng, A* 133:577–580
- [77] Gránásy L, Tegze M (1991) Crystal–melt interfacial free energy of elements and alloys. *Mater Sci Forum* 77:243–256
- [78] Spaepen F (1994) Homogeneous nucleation and the temperature dependence of the crystal interfacial tension. *Solid States Phys* 47:1–32
- [79] Jiang Q, Shi HX, Zhao M (1999) Free energy of crystal–liquid interface. *Acta Mater* 47:2109–2112
- [80] Kaptay G (2001) A model for the solid–liquid interfacial energies of pure metals. *Trans Join Weld Res Inst* 30(Special Issue):245–250
- [81] Jian Z, Kuribayashi K, Jie W (2002) Solid–liquid interface energy of metals at melting point and undercooled state. *Mater Trans* 43:721–726
- [82] Kaptay G (2005) Modeling interfacial energies in metallic systems. *Mater Sci Forum* 473–474:1–10
- [83] Jian Z, Li N, Zhu M, Chen J, Hang FC, Jie W (2012) Temperature dependence of the crystal–melt interfacial energy of metals. *Acta Mater* 60:3590–3603
- [84] Zhou H, Lin X, Wang M, Huang W (2013) Calculation of crystal–melt interfacial free energies of fcc metals. *J Cryst Growth* 366:82–87
- [85] Owolabi TO, Akande KO, Olatunji SO (2016) Computational intelligence method of estimating solid–liquid interfacial energy of materials at their melting temperatures. *J Intell Fuzzy Systems* 31:519–527
- [86] Eustathopoulos N, Joud J-C, Desre P (1972) Etude thermodynamique de la tension interfaciale solide/liquide pour un système métallique binaire. *J Chim Phys* 60:1600–1605
- [87] Eustathopoulos N, Joud J-C, Desre P (1974) Etude thermodynamique de la tension interfaciale solide/liquide pour un système métallique binaire. *J Chim Phys* 71:777–787
- [88] Warren R (1980) Solid–liquid interfacial energies in binary and pseudo-binary systems. *J Mater Sci* 15:2489–2496. <https://doi.org/10.1007/BF00550752>
- [89] Camel D (1980) Chemical adsorption and temperature dependence of the solid–liquid interfacial tension of metallic binary alloys. *Acta Metall* 28:239–247
- [90] Chatain D, Pique D, Coudurier L, Eustathopoulos N (1985) Calculation of the solid–liquid interfacial tension in metallic ternary systems. *J Mater Sci* 20:2233–2244. <https://doi.org/10.1007/BF01112309>
- [91] Shimizu I, Takei Y (2005) Thermodynamics of interfacial energy in binary metallic systems: influence of adsorption on dihedral angles. *Acta Mater* 53:811–821
- [92] Lippmann S, Jung IH, Paliwal M, Rettenmayr M (2016) Modelling temperature and concentration dependent solid/liquid interfacial energies. *Philos Mag* 96:1–14
- [93] Bonissent A, Mutaftschiev B (1977) A computer built random model for simulation of the crystal–melt interface. *Philos Mag* 35:65–73
- [94] Luo SN, Ahrens TJ, Cagin T, Strachan A, Goddard WA III, Swift DC (2003) Maximum superheating and undercooling: systematics, molecular dynamics simulations, and dynamic experiments. *Phys Rev B* 68:134206
- [95] Wu L, Xu B, Li Q, Liu W (2015) Anisotropic crystal–melt interfacial energy and stiffness of aluminum. *J Mater Res* 30:1827–1835
- [96] Xia Y, Li CH, Luan YW, Han XJ, Li JG (2016) Molecular dynamics studies on the correlation of undercoolability and thermophysical properties of liquid Ni–Al alloys. *Comp Mater Sci* 112:383–394
- [97] Liu S, Wang Z, Shi Z, Zhou Y, Yang Q (2017) Experiments and calculations on refining mechanism of NbC on primary M7C3 carbide in hypereutectic Fe–Cr–C alloy. *J Alloys Compd* 713:108–118
- [98] Qi C, Xu B, Kong LT, Li JF (2017) Solid–liquid interfacial free energy and its anisotropy in the Cu–Ni binary system investigated by molecular dynamics simulations. *J Alloys Compd* 708:1073–1080
- [99] Kaptay G (2012) On the interfacial energy of coherent interfaces. *Acta Mater* 60:6804–6813
- [100] Butler JAV (1932) The thermodynamics of the surfaces of solutions. *Proc R Soc A* 135:348–375
- [101] Kaptay G (2005) A method to calculate equilibrium surface phase transition lines in monotectic systems. *Calphad* 29:56–67 and 262
- [102] Mekler C, Kaptay G (2008) Calculation of surface tension and surface phase transition line in binary Ga–Tl system. *Mater Sci Eng, A* 495:65–69
- [103] Costa C, Delsante S, Borzone G, Zivkovic D, Novakovic R (2014) Thermodynamic and surface properties of liquid Co–Cr–Ni alloys. *J Chem Thermod* 69:73–84
- [104] Brillo J, Kolland G (2016) Surface tension of liquid Al–Au binary alloys. *J Mater Sci* 51:4888–4901. <https://doi.org/10.1007/s10853-016-9794-x>
- [105] Jha IS, Khadka R, Koirala RP, Singh BP, Adhikari D (2016) Theoretical assessment on mixing properties of liquid Ti–Na alloys. *Philos Mag* 96:1664–1683

- [106] Pelegrina JL, Gennari FC, Condó AM, Guillemet AF (2016) Predictive Gibbs-energy approach to crystalline/amorphous relative stability of nanoparticles: size effect calculations and experimental test. *J Alloys Compd* 689:161–168
- [107] Wessing JJ, Brillo J (2017) Density, molar volume, and surface tension of liquid Al–Ti. *Metall Mater Trans A* 48:868–882
- [108] Kim Y, Kim HG, Kang Y-B, Kaptay G, Lee JH (2017) Prediction of phase separation in immiscible Ga–Ti alloys. *Metall Mater Trans A* 48A:2701–2705
- [109] Kaptay G (2015) On the partial surface tension of components of a solution. *Langmuir* 31:5796–5804
- [110] Korozs J, Kaptay G (2017) Derivation of the Butler equation from the requirement of the minimum Gibbs energy of a solution phase, taking into account its surface area. *Coll Surf A* 533:296–301
- [111] Brillo J, Schmid-Fetzer R (2014) A model for the prediction of liquid–liquid interfacial energies. *J Mater Sci* 49:3674–3680. <https://doi.org/10.1007/s10853-014-8074-x>
- [112] Weltsch Z, Lovas A, Takács J, Cziráki Á, Tóth A, Kaptay G (2013) Measurement and modelling of the wettability of graphite by a silver–tin (Ag–Sn) liquid alloy. *Appl Surf Sci* 268:52–60
- [113] Kaptay G (2016) Modeling equilibrium grain boundary segregation, grain boundary energy and grain boundary segregation transition by the extended Butler equation. *J Mater Sci* 51:1738–1755. <https://doi.org/10.1007/s10853-015-9533-8>
- [114] Tallon JL (1980) The entropy change on melting of simple substance. *Phys Lett A* 76:139–142
- [115] Kaptay G (2008) A unified model for the cohesive enthalpy, critical temperature, surface tension and volume thermal expansion coefficient of liquid metals of bcc, fcc and hcp crystals. *Mater Sci Eng, A* 495:19–26
- [116] Topuridze NI, Hantadze DV (1978) Uchot geometricheskogo faktora pri raschote izbitochnogo obioma rastvora. *Zh Fiz Himii LII* 81–84
- [117] Lemaignan C (1980) Hard spheres simulation of the size effect in liquid and amorphous metallic alloys. *Acta Metall* 28:1657–1661
- [118] Liu S, Napolitano RE, Trivedi R (2001) Measurement of anisotropy of crystal–melt interfacial energy for a binary Al–Cu system. *Acta Mater* 49:4271–4276
- [119] Kaptay G (2015) Approximated equations for molar volumes of pure solid fcc metals and their liquids from zero Kelvin to above their melting points at standard pressure. *J Mater Sci* 50:678–687. <https://doi.org/10.1007/s10853-014-8627-z>
- [120] Emsley J (1989) *The Elements*. Clarendon Press, Oxford
- [121] Engin S, Büyük U, Marasli N (2009) Determination of interfacial energies in the Al–Ag and Sn–Ag alloys by using Bridgman type solidification apparatus. *J Alloys Compd* 488:138–143
- [122] Massalski TB (ed) (1990) *Binary alloy phase diagrams*, vol 3, 2nd edn. ASM International, Materials Park, Ohio, USA
- [123] Witusiewicz VT, Hecht U, Fries SG, Rex S (2005) The Ag–Al–Cu system. I. Reassessment of the constituent binary system. *J Alloys Compd* 385:133–143
- [124] Ansara I, Dupin N, Lukas HL, Sundman B (1997) Thermodynamic assessment of the Al–Ni system. *J Alloys Compd* 247:20–30
- [125] Bulla A, Carreno-Bodensiek C, Pustal B, Berger R, Buhrig-Polaczek A, Ludwig A (2007) Determination of the solid–liquid interface energy in the Al–Cu–Ag system. *Metall Mater Trans A* 38A:1956–1964
- [126] Keslioglu K, Ocak Y, Aksöz S, Marasli N, Cadirli E, Kaya H (2010) Determination of interfacial energies for solid Al solution in equilibrium with Al–Cu–Ag liquid. *Met Mater Int* 16:51–59
- [127] Witusiewicz VT, Hecht U, Fries SG, Rex S (2005) The Ag–Al–Cu system II. A thermodynamic evaluation of the ternary system. *J Alloys Compd* 387:217–227